Engineering Structures 132 (2017) 456–470

Contents lists available at ScienceDirect

Engineering Structures

journal homepage: www.elsevier.com/locate/engstruct

Uncertainty quantification in the dynamics of a guyed mast subjected to wind load

Jorge S. Ballaben [a], Rubens Sampaio [b], Marta B. Rosales [a,*]

[a] Department of Engineering, Universidad Nacional del Sur, Alem 1253, 8000 Bahía Blanca and CONICET, Argentina
[b] Pontificia Universidade Católica, Department of Mechanical Engineering, Rua Marquês de São Vicente, 225, 22452-900 Rio de Janeiro, Brazil

ARTICLE INFO

Article history:
Received 20 May 2015
Revised 8 September 2016
Accepted 10 November 2016

Keywords:
Guyed mast
Wind loads
Nonlinear dynamics
Uncertainty quantification

ABSTRACT

A study of the stochastic dynamics of a guyed mast under wind action is reported in the present work. The simplified structural model consists of a beam-column accounting for the second order effect due to axial loads and one inclined guy which is represented by a nonlinear extensible cable. The governing system is discretized with finite elements and a reduced order model is afterwards constructed using a basis of vibration modes.

Both, the load and the structural model are considered stochastic. The wind load is derived from a wind velocity field after the application of the Spectral Representation Method. Since nonlinear structures show special sensitivity to dynamic loads, the reference nominal wind velocity (suggested by the codes) is also considered a random parameter. The guy pretension is a significant parameter in the behavior of guyed structures and its variation is a relevant issue. Furthermore, the bending stiffness can vary due to the structure reinforcements. Since it is not easy to foresee their behavior, an uncertainty quantification study appears necessary.

After performing Monte Carlo simulations, the outcomes are evaluated accounting for each statistical parameter (guy tension, bending stiffness and wind nominal velocity) separately. Also, parameters combinations are studied. Six illustrative cases are reported. The results are shown in different ways (probability distribution functions (PDFs), correlation, exceeding limits, etc.). The stochastic variables have different effects on the statistics of the dynamic response. The guy pretension and the nominal wind velocity are found to be the most influential random quantities. Despite the potential of adverse impact, detailed studies of guyed structures under natural actions, as wind or earthquake, are not frequent. The involved variables are usually uncertain and it can be concluded that an uncertainty quantification study leads to a more realistic approach of the dynamic behavior of the structural system, in particular regarding the sensitivity to some parameters.

© 2016 Elsevier Ltd. All rights reserved.

1. Introduction

Guyed masts are extensively employed, *e.g.* from simple masts to more complex structures, to support devices such as antennas for radio, TV and other types of communication as well as ancillaries (Fig. 1a). This structural typology has clear advantages in the open country, where there are no restrictions on the position of the cable anchors. However, it can also be found in urban areas, due to its low cost compared with other typologies.

Despite the large potential of adverse impact (*e.g.* fatigue of structural members or affected quality of the transmission in communication guyed towers), dynamic actions as wind and earthquakes are not addressed in detail with exception of special cases (e.g. [1–4]).

Other authors' works show that guyed structures have special sensitivity to the type and amplitude of the excitation [5–7], even avoiding the resonance effects. After the derivation of the equations of motion of a cable-stayed beam, the in-plane and out-of-plane eigenvalue problems are solved by Wang et al. [8]. Also, nonlinear modes are studied along with the contribution of the coupling term. Then, a stochastic study appears appropriate not only due to the random wind load but also to the randomness of some relevant structural parameters.

A study on this regard, related to mechanical systems is reported by Bellizzi and Sampaio [9]. The smooth decomposition method combined with the Petrov-Galerkin projection for

* Corresponding author.
E-mail addresses: jorgeballaben@gmail.com (J.S. Ballaben), rsampaio@puc-rio.br (R. Sampaio), mrosales@criba.edu.ar (M.B. Rosales).

http://dx.doi.org/10.1016/j.engstruct.2016.11.025
0141-0296/© 2016 Elsevier Ltd. All rights reserved.

Nomenclature

$\bar{a}$	coefficient (Appendix A)
c	relative damping coefficient
$\bar{c}$	coefficient (Appendix A)
$\bar{d}$	coefficient (Appendix A)
$f^0(t)$	Gaussian stationary random process
f_L	nondimensional frequency
f_X	probability density function of the random variable X
i	subindex, c (cable), b (beam)
k_d	wind direction factor
k_{zt}	topographic factor
l_i	structural element length
m_i	mass per unit length
$\bar{m}_i$	coefficient (Appendix A)
$\bar{p}$	coefficient (Appendix A)
$\mathbf{q}$	modal amplitude vector
q_z	wind pressure
$\bar{q}_z$	wind pressure including $u(z,t)$
t	time variable
$u(z,t)$	fluctuating wind velocity
u_i	axial displacement
v_i	transverse displacement
x_i	spatial variable
z	mast length variable
z_g	roughness parameter
A_f	exposed area of mast
A_i	cross-sectional area
A_t	exposed area of mast without holes
C_f	shape parameter
C_z	coherence coefficient
E	modulus of elasticity
D	displacement
$\bar{D}$	cable sag
F	wind load magnitude
F_j	force per unit length
G	gust factor
H	chord component of T
$\mathbf{H}(\omega_n)$	Cholesky transform of $S^0(\omega)$
I	importance factor
I_b	second moment of area of the cross-section
L_c	length of cable chord
L_u	length scale of turbulence
P_H	guy force component along the mast axis direction
R_N	normalized power spectrum
S	entropy (information theory)
$S^0(\omega)$	cross-spectral density matrix
T	cable pretension force
$U(z)$	mean wind velocity
V	reference wind velocity
V_n	nominal wind velocity
Y_c	cable initial configuration
$\mathcal{C}$	damping operator
$\mathcal{F}$	force operator
$\mathcal{K}_{\mathcal{L}}$	linear stiffness operator
$\mathcal{K}_{\mathcal{NL}}$	nonlinear stiffness operator
$\mathcal{BC}$	boundary conditions operator
α	power law parameter
ϵ_c	elongation of the cable
Φ_{kn}	random phase angles
ψ_{kn}	random values
σ	standard deviation
$\Delta\omega$	frequency interval
Φ	admissible function
H	random cable pretension
I	random moment of second order of the mast cross-section
V_n	random nominal velocity

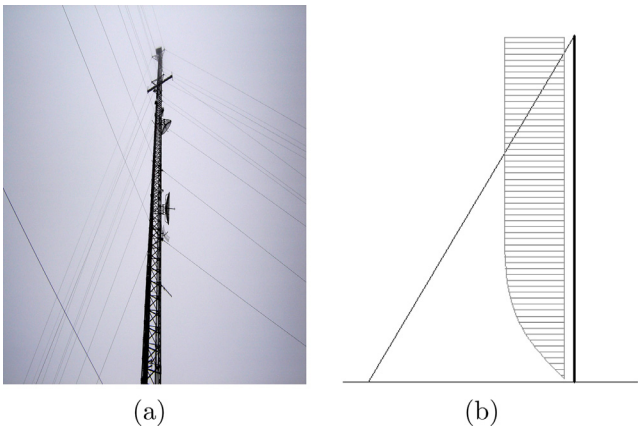

Fig. 1. Guyed mast. (a) Typical guyed tower for mobile signal transmission; (b) reduced model under study.

structure-preserving model reduction is used to analyze second-order discrete nonlinear structural systems under random excitation. Nonlinear mechanical systems under random excitation with homogeneous and non-homogeneous mass distribution were considered.

In the present study, the stochastic dynamics of a guyed mast is analyzed under wind load action. The simplified structural model consists of a beam-column accounting for the second order effect due to axial loads and one inclined guy (Fig. 1b). The analyzed system includes a stochastic load and also a stochastic structural model through random parameters.

Since the wind load contains energy that interacts with flexible structures, the dynamic response becomes important in the analysis of guyed masts. The mast acts strongly in a nonlinear fashion when the guys vary between slack and taut states.

The wind load is variable in space and time (during an event) and it changes from one event to the other. Hence, a study considering the wind load as a stochastic event, and the analysis of the response of the structure to a variety of events with different nominal velocities (that can be considered stochastic as well), is desirable to understand the behavior of the structural system.

Although the guy pretension is determined at the design stage, it can change during the construction procedure and also along the structure service life with respect to the design value, affecting the system performance and even its stability [10]. As the guy pretension is a significant parameter of the structure, its variation is a relevant issue and the introduction of uncertainty appears adequate.

Also, the column-beam stiffness can be a variable value. For example, various companies can share the use of one structure to install their antennas; this situation requires, in most of the cases, the retrofit of the mast and one strategy consists in the total or partial reinforcement of the legs of the lattice mast. However, the stiffness of the reinforced mast is uncertain due to the construction procedures. Thus, a stochastic treatment of the mast bending stiffness seems indicated.

The fluctuating component of the wind velocity is obtained through the Spectral Representation Method (SRM) [11] starting from a given Power Spectral Density function (*psdf*) [12]. The temporal and spatial correlations are taken into account by finding the cross-spectrum and introducing a coherence function. The method yields a temporal record of the fluctuating wind velocity. Combined with the standard recommendations, the fluctuating wind pressure is applied along the mast height.

Miguel et al. [13] used this load approach to evaluate in detail the dynamic response of a transmission line. The authors considered different models for the power spectra of the fluctuating wind velocity components as well as for the correlation functions. The only source of uncertainty is the wind load and they suggest the need of including uncertainties in the structure idealization.

In the present study and using the classical extended Hamilton's principle, the equations of motion that govern the transverse vibration of the system are obtained. The nonlinear model of the cable follows the approach reported by Gattulli and Lepidi [14]. Then, and after the statement of the weak form, the governing system is discretized by finite elements.

A similar approach is used by Shi and Salim [15] to study the static and dynamic response of guyed masts. Since the FEM approximation of the complete model in dynamic nonlinear analysis is computationally expensive, the need for a formulation of a further reduced model for uncertainty quantification studies, is apparent. Next, the linerized equations are used to perform a modal analysis of the structure. Finally, by means of a Galerkin projection, the main nonlinear PDE system is reduced to a 2-DOF model, using two selected normal modes extracted from the modal data. With this reduced order model (ROM), the nonlinear response of the structure excited by a stochastic wind load is evaluated, considering also uncertainties on the guy tension, the mast bending stiffness and the nominal wind velocity, separately and combined. A total of six cases are reported, showing the behaviors under the presence of the different random parameters.

It was found that the effect of the random quantities in the response is very dissimilar. In particular, some interesting results such as multimodalities are found for certain combinations of parameters. The guy tension and the nominal wind velocity are observed to have important effects on the dynamic response of the structure. Thus, a cautious maintenance program is needed to ensure that the guy pretension remains within a close range of the design value in order to reduce the system deflections.

2. Statement of the model

2.1. Model description

The plane configuration of a guyed column (see Fig. 2) is described, referenced to the static equilibrium state, by the cable displacement components $u_c(x_c,t)$ and $v_c(x_c,t)$ along the abscissa x_c, and by the beam-column transverse displacements $v_b(x_b,t)$ and $u_b(x_b,t)$ along x_b.

The following assumptions are made: (a) both the cable and the beam-column are considered as homogeneous one-dimensional elastic continua obeying a linear stress-strain relationship; (b) the equilibrium configuration for the inclined cable is described through a quadratic parabola under the assumptions of small sag to length ratio; (c) axial extensions of the cable are described by the Lagrangian strain of the centerline; (d) the flexural, torsional and shear stiffness of the cable are negligible; (e) the torsional and shear strain of the beam-column are negligible; (f) the nonlinearity of the problem arises from the cable formulation; (g) a second order effect due of the axial load (assumed constant) is accounted for in the beam-column equation. The cable formulation

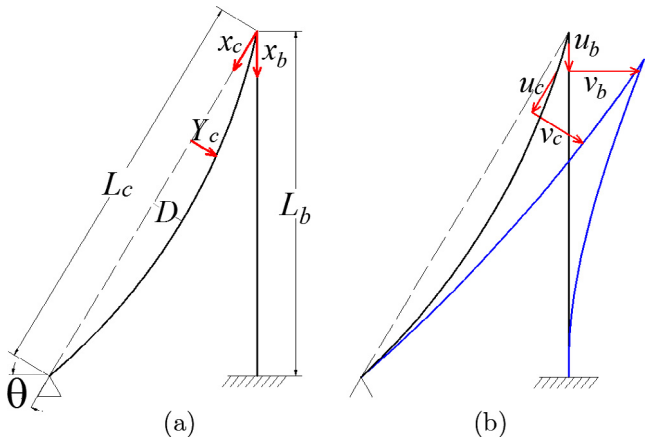

Fig. 2. Cable-stayed tower configurations: (a) static; (b) dynamic.

follows the approach reported in [14]. Under these assumptions and using the classical extended Hamilton's principle, the equations of motion governing the transverse vibration of the guyed column are obtained:

$$\begin{aligned}
&v_b : m_b\ddot{v}_b + c_b\dot{v}_b + EIv_b'''' + P_H v_b'' = F_{v_b}(t,x_b)\\
&u_b : m_b\ddot{u}_b + c_b\dot{u}_b + EA_b u_b'' = F_{u_b}(t,x_b)\\
&v_c : m_c\ddot{v}_c + c_c\dot{v}_c - [Hv_c' + EA_c(Y_c' + v_c')\epsilon_c]' = F_{v_c}(t,x_c)\\
&u_c : m_c\ddot{u}_c + [EA_c\epsilon_c]' = F_{u_c}(t,x_c)
\end{aligned} \tag{1}$$

with the following set of geometric and natural boundary conditions:

$$\begin{aligned}
&u_c(L_c) = v_c(L_c) = 0\\
&v_b(L_b) = v_b'(L_b) = u_b(L_b) = 0\\
&EIv_b''(0) = 0\\
&v_b(0) = -u_c(0)\cos\theta + v_c(0)\sin\theta\\
&u_b(0) = u_c(0)\sin\theta + v_c(0)\cos\theta\\
&EIv_b'''(0) + (EA_c\epsilon_c + H)\cos\theta +\\
&\quad [EA_c\epsilon_c(Y_c'(0) + v_c'(0)) + Hv_c'(0)]\sin\theta = 0
\end{aligned} \tag{2}$$

Here $(*)' = d(*)/dx_c$ and $\dot{(*)} = d(*)/dt$, m_b and m_c denote the beam and cable mass per unit length, respectively, $EI = E_bI_b$ is the beam flexural stiffness, P_H is the component of the force in the direction of the mast, $EA_c = E_cA_c$ and $EA_b = E_bA_b$ are the cable and beam axial stiffness, respectively, H is the component along the chord of the mean static cable pretension T in the cable (due to the small slope, H and T are practically equal) and F_{v_b}, F_{u_b}, F_{v_c} and F_{u_c} are generic external loads. Y_c is the initial configuration of the cable and, due the hypothesis of small sag ($\bar{D}$) to span ratio, $Y_c(x_c) = 4\bar{D}(x_c/L_c - (x_c/L_c)^2)$. Finally, $\epsilon_c = u_c + Y_c'v_c' + 1/2\,v_c'^2$ is the elongation of the cable. Since in cable-stayed structures the beam and the cable materials can generally have different viscous behavior, the model accounts separately for the damping per unit length, c_b and c_c, respectively. An estimate of the system damping is assumed to give the conventional values $c_i = 8.5\times10^{-3}(2m_i\omega_i)$, with $i = c,b$ and ω_i is a natural frequency of the system. Here ω_i is chosen by observation of the modal shapes used in the approximation, *i.e.* if the modal shape selected is a cable-like mode, then the corresponding frequency is used for the damping term of the cable; the values of ω_i were found with $I_b = 8.33\times10^{-4}$ m^4.

The assumed values of the constants for the present problem are detailed in Table 1.

Table 1
Values of the constants for Eqs. (1) and (2).

l_b (m)	E_b (10^{11} N/m^2)	$I_b = I$ (10^{-4} m^4)	A_b (m)^2	m_b (kg)	l_c (m)	E_c (10^{11} N/m^2)	A_c (10^{-5} m)^2	m_c (kg)	H (N)
30	2.1	4.16–13	0.04	314	32.31	1.5	7.854	0.61	7000–14,000

2.2. Weak formulation and finite element discretization

The weak formulation of the system Eqs. (1) and (2) writes as

$$\mathcal{M}(\ddot{v},\phi)+\mathcal{C}(\dot{v},\phi)+\mathcal{K}_L(v,\phi)+\mathcal{K}_{NL}(v,\phi)+\mathcal{BC}(v,\phi)=\mathcal{F}(v,\phi), \tag{3}$$

where $\mathcal{M},\mathcal{C},\mathcal{F}$ are the mass, damping and external force operators respectively. $\mathcal{K}_L$ and $\mathcal{K}_{NL}$ are the linear and nonlinear stiffness operators and $\mathcal{BC}$ is the boundary condition operator. ϕ denotes the admissible functions.

$$\mathcal{M}(\ddot{v},\phi)=\int_0^{l_b} m_b(\ddot{v}_b\phi_b+\ddot{u}_b\phi_b)dx_b+\int_0^{l_c} m_c(\ddot{v}_c\phi_c+\ddot{u}_c\phi_c)dx_c \tag{4a}$$

$$\mathcal{C}(\dot{v},\phi)=\int_0^{l_b} c_b(\dot{v}_b\phi_b+\dot{u}_b\phi_b)dx_b+\int_0^{l_c} c_c(\dot{v}_c\phi_c+\dot{u}_c\phi_c)dx_c \tag{4b}$$

$$\mathcal{F}(v,\phi)=\int_0^{l_b}(F_{u_b}\phi_b+F_{v_b}\phi_b)dx_b+\int_0^{l_c}(F_{v_c}\phi_c+F_{u_c}\phi_c)dx_c \tag{4c}$$

$$\begin{aligned}\mathcal{K}_L(v,\phi)=&\int_0^{l_b}\left(EI_b v_b''\phi_b''-P_H v_b'\phi_b'+EA_b u_b'\phi_b'\right)dx_b\\&+\int_0^{l_c}(Hv_c'\phi_c'+EA_c u_c'\phi_c')dx_c\end{aligned} \tag{4d}$$

$$\mathcal{K}_{NL}(v,\phi)=\int_0^{l_c} EA_c\left[(Y_c'+v_c')\left(u_c'+Y_c'v_c'+\frac{v_c'^2}{2}\right)\phi_c'+\left(Y_c'v_c'+\frac{v_c'^2}{2}\right)\phi_c'\right]dx_c, \tag{4e}$$

$$\begin{aligned}\mathcal{BC}(v,\phi)=&\left[Hv_c'+EA_c(Y_c'+v_c')(u_c'+Y_c'v_c'+v_c'^2/2)\right]\phi_c|_0^{l_c}\\&+EA_c(u_c'+Y_c'v_c'+v_c'^2/2)\phi_c|_0^{l_c}+EI_b v_b''\phi_b|_0^{l_b}-EI_b v_b''\phi_b'|_0^{l_b}\\&+P_H v_b'\phi_b|_0^{l_b}+EA_b u_b'\phi_b|_0^{l_b}\end{aligned} \tag{4f}$$

in which ϕ_b and ϕ_c stand for the beam and cable admissible functions respectively. P_H is the guy force component in the mast axis direction. After stating the weak formulation for the guyed column, the system is discretized by means of an *ad hoc* finite element formulation. The column is modeled using a two nodes, 6-DOF (transverse and axial displacements and slope at each node) beam element and the cable using a three nodes, 6-DOF (axial and transverse displacements at each node) cable element. After a linearization of the system, the natural frequency problem was solved. Fig. 3 depicts three selected modal shapes found with the modal analysis. Some modes are global and others, cable-like or beam-like.

2.3. Galerkin projection and reduced order model (ROM)

By means of a Galerkin projection, the main nonlinear equations system is further reduced to a 2-DOF model, using two selected normal modes extracted from the previous modal analysis. The nonlinear response of the structure excited by a stochastic wind load is evaluated using this ROM, considering also uncertainties of the initial pretension on the guy, the bending stiffness and the nominal wind velocity. The two-order ROM was previously verified with a finite element model within the commercial software ALGOR [16] and it was found that it reproduces acceptably the amplitude, shape and frequency as seen in Fig. 4. The small shift of around 1% in the main frequency is thought to be related mainly to the differences in the damping model used in the models. In effect, the 2 DOF ROM is compared with a finite element model. The first one is simpler but the cable is represented by a nonlinear formulation. On the other hand, the second model contains truss elements to describe the guy. In any case, the model is calibrated with the damping coefficient.

The displacements have been expressed in the modal space as $v=\Phi\mathbf{q}$. The displacement vector is $v=\{v_b(x_b,t),u_b(x_b,t),v_c(x_c,t),u_c(x_c,t)\}^T$ and the modal matrix is $\Phi=[\phi_\mathbf{1}|\phi_\mathbf{2}]$ which is composed by the eigenfunctions $\phi_\mathbf{i}=\{\phi_{b_vi}(x_b),\phi_{b_ui}(x_b),\phi_{v_ci}(x_c),\phi_{u_ci}(x_c)\}^T$ and the modal amplitude vector is $\mathbf{q}=\{q_1(t),q_2(t)\}^T$. After imposing the stationarity of the associated Hamiltonian, the following nonlinear ordinary differential equations in terms of the generalized coordinates q_1 and q_2 are obtained:

$$\begin{aligned}&\bar{m}_1\ddot{q}_1+\bar{a}_1\dot{q}_1+\bar{c}_1q_1+\bar{c}_2q_2+\bar{c}_{12}q_1q_2+\bar{c}_{11}q_1^2+\bar{c}_{22}q_2^2+\bar{c}_{211}q_1^2q_2+\\&\bar{c}_{122}q_1q_2^2+\bar{c}_{111}q_1^3+\bar{c}_{222}q_2^3=\bar{p}_1(t)\end{aligned} \tag{5}$$

$$\begin{aligned}&\bar{m}_2\ddot{q}_2+\bar{a}_2\dot{q}_2+\bar{d}_1q_1+\bar{d}_2q_2+\bar{d}_{12}q_1q_2+\bar{d}_{11}q_1^2+\bar{d}_{22}q_2^2+\bar{d}_{211}q_1^2q_2+\\&\bar{d}_{122}q_1q_2^2+\bar{d}_{111}q_1^3+\bar{d}_{222}q_2^3=\bar{p}_2(t).\end{aligned} \tag{6}$$

The coefficients of Eqs. (5) and (6) are included in Appendix A.

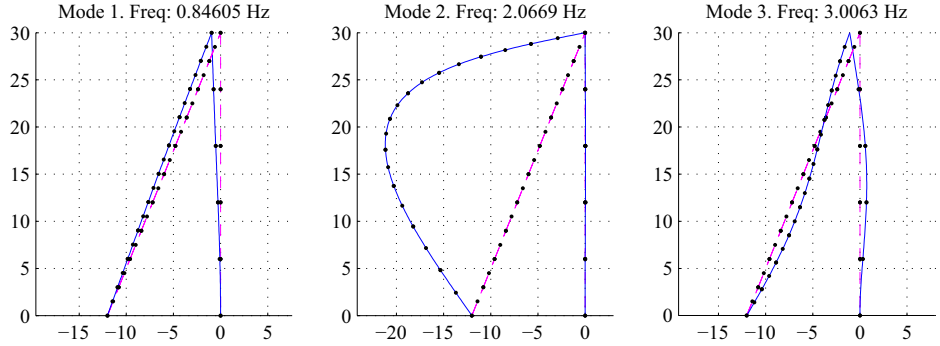

Fig. 3. Mode shapes of the guyed mast.

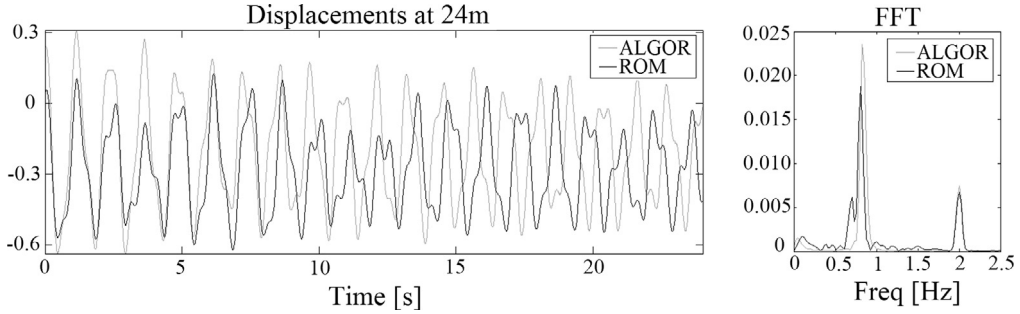

Fig. 4. Verification of the ROM model. Comparison with a finite element model (ALGOR [16]).

3. Wind load

In order to simulate typical load conditions, three loads were taken into account: weight (gravitational load), pre-stress on the cable and a transverse wind load on the column (Fig. 1b). A usual approach to represent the wind action on a structure is to separate it in the mean and the fluctuating component of the wind velocity. The wind load is found after converting the wind velocity into a quasi-static pressure and affected by several coefficients indicated in the different code standards. Here, the fluctuating wind velocity is found through the Spectral Representation Method (SRM) first proposed in [11]. This methodology starts from a spectral representation in the frequency domain of the wind velocity and leads to a function in the time domain, that accounts for both the temporal and spatial correlations.

The method uses a power density spectrum and a coherence function. Then, the random signals are created as a superposition of harmonic functions, weighted by coefficients that account for the importance of the each frequency value within the spectrum and the spatial correlation. The power density function is discretized in regular intervals and the frequencies used in the harmonic functions are chosen randomly within each interval, in order to avoid a harmonic result.

Next, the method will be introduced theoretically and then, its implementation will be described. The power density function employed in the present work is the one proposed by Davenport (see, for instance, [12]). The height variation of the velocity follows the procedure of the Argentinian standard [17].

3.1. Spectral Representation Method

Following the methodology developed in [11], let us consider a set of m Gaussian stationary random processes $f_j^0(t),\ j = 1,2,\ldots,m$, with zero mean $E[f_j^0(t)] = 0$, with a cross-spectral density matrix $S^0(\omega)$.

After skipping some steps that can be found in [11], the $f_j^0(t)$ process can be simulated by the following series,

$$f_j(t) = \sum_{k=1}^{m}\sum_{n=1}^{N}|H_{jk}(w_n)|\sqrt{2\Delta\omega}\cos[\hat{\omega}_n t + \theta_{jk}(w_n) + \Phi_{kn}] \tag{7}$$

where $\Delta\omega$ is the frequency interval with which the power spectrum density function is discretized, $w_n = \Delta\omega(n-1)$, $\hat{\omega}_n = w_n + \psi_{kn}\Delta\omega$, ψ_{kn} are random values uniformly distributed between 0 and 1, N is the amount of frequency ranges, Φ_{kn} are the random independent phase angles uniformly distributed between 0 and 2π.

It can be shown that the process $f_j(t),\ j = 1,2,\ldots,m$ simulated by Eq. (7) produces the desired cross-correlation function and the spectral density with respect to the group mean.

3.2. SRM implementation to derive the time dependent wind velocity field

In order to model the fluctuating component of the wind velocity, the implementation of the SRM is next detailed. The first step is to choose a power spectral density function (*psdf*) and a coherence function. In this work, the *psdf* suggested for Davenport [12] is used,

$$R_N(z,\omega) = \frac{wS(z,\omega)}{\sigma^2(z)} = 2/3\,\frac{f_L^2}{(1+f_L^2)^{4/3}} \tag{8}$$

where ω is the frequency in Hz, σ is the standard deviation, z is the height of the analyzed point and f_L is the non-dimensional frequency:

$$f_L = \omega\frac{L_u}{U(z)}. \tag{9}$$

L_u is the length scale of turbulence (1200 m for the Davenport model) and $U(z)$ is the height dependent value of mean wind mean velocity. The expression for $U(z)$ corresponds to the potential law adopted by the Argentinian standard [17]

$$U(z) = 2.01V(z/z_g)^{2/\alpha} \tag{10}$$

in which z is the height of the analyzed point, V is the reference wind velocity which, together with z_g and α, are values given by the standard code for the location of the structure and will be explained in Section 3.3. The coherence function is

$$Coh(z_i,z_j,\omega) = exp\left\{-2\omega\frac{C_z|z_i - z_j|}{U(z_i)+U(z_j)}\right\} \tag{11}$$

where z_i and z_j are the heights of two given points in the mast. Then, each S_{ij} of the $S(\omega)$ matrix, for a given value of frequency can be calculated as:

$$S_{ij}(z_i,z_j,\omega) = \sqrt{S(z_i,\omega)S(z_j,\omega)}Coh(z_i,z_j,\omega) \tag{12}$$

Following these procedure, N matrices can be created, one for each frequency value.

Following the procedure suggested by [11], it is possible to construct the temporal series given by

$$u(z_j,t) = \sum_{k=1}^{m}\sum_{n=1}^{N}H_{jk}(w_n)\sqrt{2\Delta\omega}\cos[2\pi\hat{\omega}_n t + \Phi_{kn}] \tag{13}$$

in which $H_{jk}(w_n)$ is used instead of $|H_{jk}(w_n)|$ and $\theta_{jk}(w_n)$ is neglected because only the real part of the *psdf* is taken into account. The maximum frequency of the spectrum was assumed $w_c = 2.5$ Hz. The frequency interval $\Delta\omega$ was selected as 0.004 Hz. The time interval required to generate the function of Eq. (13) is $\Delta t \leqslant 1/2w_c$. The value adopted in this work is $\Delta t = 0.20$ s. The mast height was dis-

Table 2
Coefficients used for the calculation of the time dependent velocity field.

Coefficient	σ^2	L_u	C_z	w_c	$\Delta\omega$	Δt	N	m
Value	38.77	1200 m	11.5	2.5 Hz	0.004 Hz	0.2 s	625	12

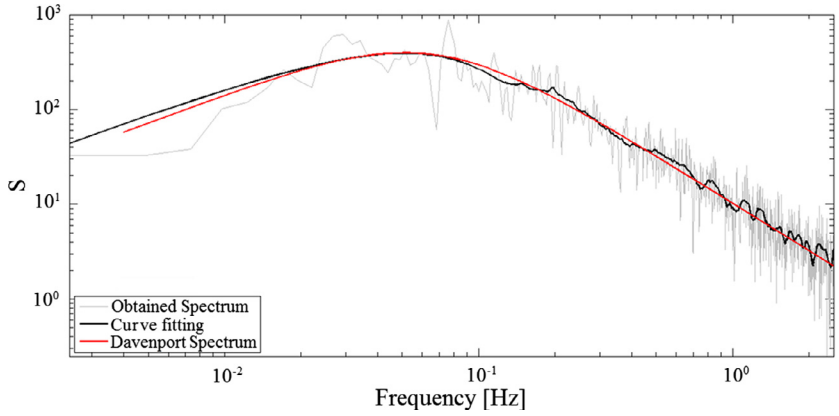

Fig. 5. Comparison of the wind velocity spectrum of the velocity series with the theoretical expression.

cretized in twelve equidistant points. Table 2 summarizes the values of the relevant parameters in order to apply the method and Fig. 5 shows the matching between the theoretical wind power spectrum with the one obtained from the Fourier transform of the cross-correlation function of two signals obtained by Eq. (13). A curve fitted to the obtained data depicts the good agreement.

3.3. Wind load derivation

In the previous section, the time dependent component of the wind velocity was derived. Next, the procedure to construct the wind load is presented. The wind load was designed following the Argentinian standard code [17] that specifies the steps for the construction of the quasi-static load. Then, it is combined with the time dependent component of the wind velocity, previously derived. Some modifications are introduced in order to take into account the dynamics of the wind velocity, modeled by Eq. (13). The standard defines the static wind load as

$$F = q_z G C_f A_f \tag{14}$$

where F is the magnitude of the wind load, G is the gust coefficient, which takes into account the effects of the dynamic amplification and lack of correlation of loads, A_f is the exposed area of the mast, projected onto the plane normal to the loads and C_f is a coefficient which takes into account the shape of the structure, in this case, the mast.

In order to introduce the time dependent velocity the wind pressure is written as

$$\bar{q}_z = 0,613 k_{zt} k_d V(U(z) + u(z,t))I \tag{15}$$

Replacing q_z by $\bar{q}_z$ in Eq. (14),

$$F(z,t) = \bar{q}_z G C_f A_f \tag{16}$$

Table 3 shows the numerical values adopted and calculated for the coefficients.

For the sake of brevity many details were omitted. The interested reader is refered to [17] for more details.

4. Uncertainty quantification

The uncertainty quantification is performed with three parameters: one corresponding to the wind load, *i.e.* the nominal wind velocity V_n (corresponding to the deterministic parameter V_n) and the other two related to the structure itself, *i.e.* the guy tension H and the mast bending stiffness EI.

The Principle of Maximum Entropy (PME) [18,19] allows to determine the best PDF that suits with the imposed constraints, and introduces no unwarranted information, *i.e.* supplied information is equal to the removed uncertainty [20].

The PME states that, subjected to known constraints, the PDF which best represents the current state of knowledge is the one with largest entropy. PME addresses the problem in a statistically sound way. The approach is systematic and allows to handle data which is limited or coming from different sources.

The measure of uncertainty of a random variable X is defined by the following expression

$$S(f_X) = -\int_D f_X(X)\log(f_X(X))dX \tag{17}$$

in which f_X stands for the PDF of X and D is its domain. The maximization problem is frequently solved using the Lagrange's method, with a multiplier accounting for each constraint.

In the present study, no full statistical data is available for the guy tension H and the mast stiffness EI. Then, they are described by different PDFs, found under three assumptions of constraints, as follows:

1. If the only constraint are the range values of the random variable, the PME leads to a uniform PDF.

$$f(x|a,b) = \begin{cases} \frac{1}{a-b}; & a \leqslant x \leqslant b \\ 0; & \text{otherwise.} \end{cases} \tag{18}$$

2. If the range values and the mean value are known, the PME leads to a truncated exponential PDF

Table 3
Coefficients for calculating static wind loads according to [17].

Coefficient	G	A_f	A_t	C_f	I	V	k_d	k_{zt}
Value	0.85	0.57 m^2	9.41 m^2	3.13	1.00	55 m/s	0.85	1

$$f(x|\alpha) = \begin{cases} C_\alpha e^{\alpha x}; & a \leqslant x \leqslant b \\ 0; & \text{otherwise}, \end{cases} \tag{19}$$

with parameters α, a and b and where $C_\alpha = \alpha/(e^{\alpha b} - e^{\alpha a})$ and $\mu = (be^{\alpha b} - ae^{\alpha a})/(e^{\alpha b} - e^{\alpha a}) - 1/\alpha$.

3. The application of the PME under the constraints of positiveness and bounded second moment leads to a gamma PDF. The gamma distribution Eq. (20) with parameters a and b, where $E(X) = ab$; $\sigma_X^2 = ab^2$, is given by the expression:

$$f(x|a,b) = \frac{1}{b^a \Gamma(a)} x^{a-1} e^{\frac{-x}{b}}. \tag{20}$$

For V_n, a Gumbel and a Fréchet distributions are used, since that are commonly used PDFs for extreme winds. The Gumbel cumulative density function (CDF) is

$$G(v) = e^{e^{-\frac{v-M}{\beta}}}. \tag{21}$$

where two parameters are involved: M which corresponds to the median of the distribution and $\beta = (m - M)/\{\ln[-\ln(0.5)]\}$, where m is the mode of the distribution. The Fréchet CDF uses also two parameters: β is the reference velocity of the location studied (in this case $\beta = 55$ m/s) and $\gamma = 7.14$ (this value is suggested in the Argentinian Standard CIRSOC 102 [17]).

$$F(v) = e^{-\left(\frac{v}{\beta}\right)^{\gamma}}. \tag{22}$$

Afterwards, Monte Carlo simulations are performed in order to find the influence of these variables with the selected PDFs, on the structural response. To achieve significant statistical results, a convergence study on the standard deviation was first performed in each case to determine the minimum number of realizations of the Monte Carlo simulations. Fig. 6 shows the typical outcome of the convergence study. It is possible to observe that, at least, a number of 2000 realizations are necessary to achieve acceptable convergent results.

The range of values of initial pretension was chosen following the standard code suggestions [21]. Once the realizations are finished, the PDF graphs are constructed using the *ksdensity* function of MATLAB, that estimates the PDF of a set of data using the *kernel* method. The bandwidth for the kernel function (here a normal function is used), is optimized in MATLAB, and it is useful when the target PDF is normal, but can give wrong results when that condition is not fulfilled. In this work, after several tests, and following an engineering criterion, the authors adopted a bandwidth of 5 cm, that gives as result smooth PDFs and allows to observe multimodalities, when the modes are separated enough to be of engineering interest.

The efficiency of the stochastic computational model is strongly dependent on the structural model and on the statistical tools.

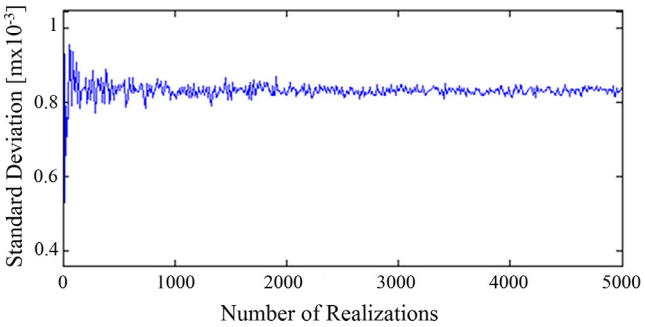

Fig. 6. Convergence study of Monte Carlo simulations. Standard deviation of the top displacements.

Regarding the first, the size and complexity condition the time in which the deterministic model is solved. On top of this, the stochastic study (in both the load and the structure) requires thousands of realizations (*i.e.* solution of the deterministic model). Even a simple and reduced model as the one stated in this work, is computing time demanding. It is known that MC is a robust technique although not the most efficient. However, the critical issue is to increase the efficiency of the deterministic model.

5. Results

Several cases were studied assuming the random variables H, EI and V_n, separately and in combinations. Cases 1 and 2 deal with the load randomness while the structural properties are considered deterministic. Case 1 is the usual problem of a deterministic structure with a stochastic load. Case 2 involves also a statistical description of the nominal wind velocity. Cases 3–7 are related to a structural stochastic model in addition to the stochastic wind load.

5.1. CASE 1. Stochastic wind load and deterministic H, EI, V_n

In this work, for sake of brevity, only results on transversal displacements of the beam are presented. The total time of calculations was 180 s. Fig. 7 depicts a sample of the transverse displacement temporal variation for the extreme cases of the initial pretension range and for $V_n = 55$ m/s. It can be seen that the overall response has smaller amplitudes for higher values of H, as expected, but also shows a very different shape. A particular frequency of vibration can be recognized at each of the depicted records, while the amplitude of the oscillation exhibits a non-periodic behavior. These observations hold for all the time history results of the displacements. A FFT study was performed to analyze the frequency content of the time history responses. Fig. 8a shows two typical FFTs, for the extreme cases of V_n and for the maximum value of H. It can be seen that for the smallest mean wind velocities, the frequency content is narrow and concentrated at one frequency (although the response is not periodic) and when the value of V_n increases, several peak frequencies appear, and their energy contents are higher. The other cases (not shown here) are intermediate between the two depicted; the range of the most important frequency content of all the cases belongs to the 0.5–0.85 Hz zone. Fig. 8b illustrates the variation of the maximum peak frequency of the FFT for all the H and V_n combinations. It can be seen that the greater variations are due the V_n parameter, although H has some relative importance.

Fig. 9 depicts the variation of the maximum and mean values of the displacements at the tip of the mast for each case of H and V_n. The parameter V_n shows a larger influence over these measures. Both Fig. 9a and b show a similar variation, despite that in Fig. 9a the results have more dependency on H but in a less predictable way. Each time history of displacements (here only the displacements at the tip of the mast are studied) can be tackled as a stochastic process, since the wind load is random itself, even assuming H, EI and V_n deterministic. In Fig. 10a, a 3D surface that depicts the evolution of the PDF of the displacements with H is shown, for a fixed value of $V_n = 70$ m/s and $EI = 1.75 \times 10^8$ N m^2. In Fig. 10b, the top view of that surface is illustrated, along with the 5% and 95% (interpolated with cubic functions) confidence bands. Fig. 10c plots some specific PDFs as examples of the various types that appear. It can be seen from Fig. 10b that the mean response is almost constant with H (the same result observed in Fig. 9b) and the width of the bands gets narrower for higher values of H. Some cases of multimodality are also observed, as the blue curve in Fig. 10c. The shape of the PDF of the displacements records

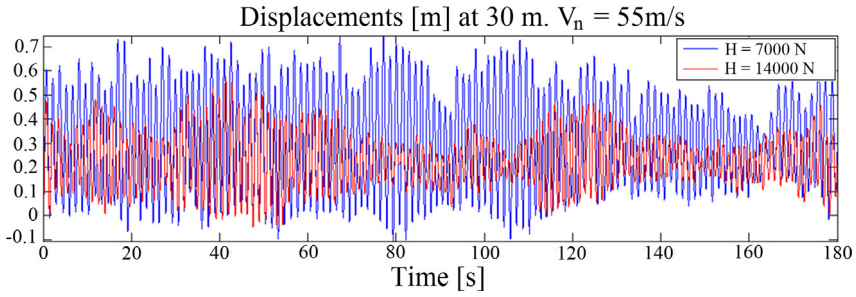

Fig. 7. Time history of the transverse displacements of the beam-column at the tip of the mast found with the deterministic reduced order model for the extreme cases of H.

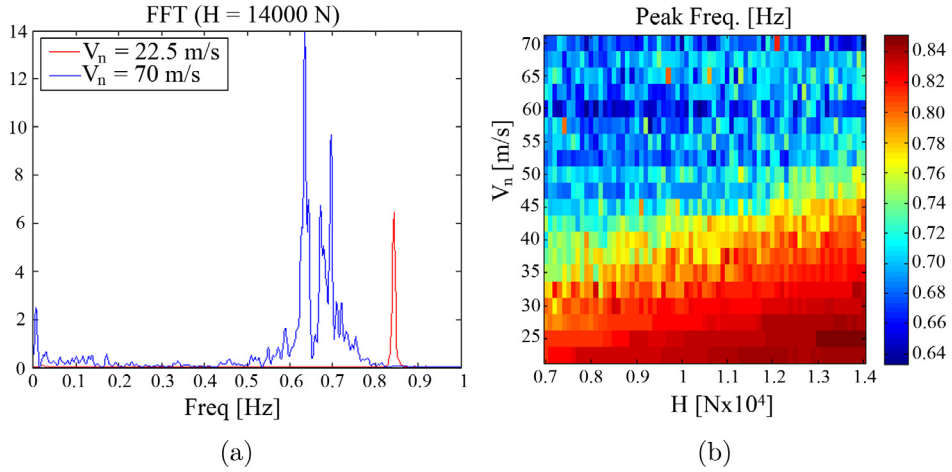

Fig. 8. Frequency analysis of the transverse displacements of the beam-column at the tip of the mast found with the deterministic structural model for all the combinations of H and V_n under stochastic wind load. (a) Two typical FFTs; (b) mosaic plot of the peak frequency.

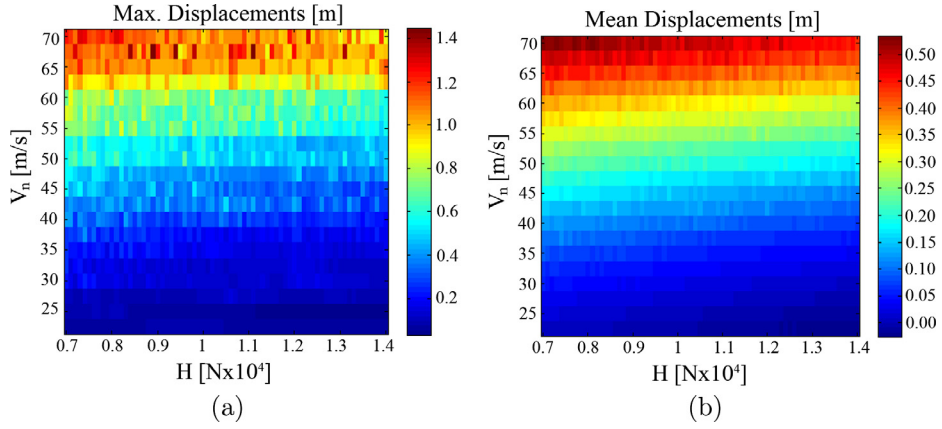

Fig. 9. Transverse displacements of the beam-column at the tip of the mast found with the deterministic structural model for all the combinations of H and V_n. (a) Maximum values; (b) mean values.

results very variable with H, ranging from pointed and centered to a flat or multimodal cases. The zones ranging from H = 7–9 kN and 12–14 kN behave as expected, since for higher values of H a decrease in the variability is apparent and the statistical response become more pointed and narrower. On the other hand, when the values of H are within the range of 9–12 kN, qualitative changes of the PDFs are found for small variations of H. Similar results were found by the authors in a previous work [22], where the dynamic is studied using a simpler approach for the loading conditions, which allows to relate the qualitative changes in the dynamic behavior with a deterministic bifurcation, present under the variation of the initial pretension. Nevertheless, the variability observed in Fig. 10 within the mid-range of values of H, is thought to be related to both the sensitivity of the model to these values of initial pretension and the nonlinear model interaction with the stochastic wind load.

Fig. 11 shows graphs similar to Fig. 10. Here, the PDF of displacements records are obtained for each value of V_n and for a fixed value of H = 7000 N. The mean and the width of the bands become higher with the value of V_n (Fig. 11b). As expected, the displacement results are more disperse - and then less predictable - for higher values of V_n, denoted by the transition from the warmer and to the colder colors (Fig. 11b). In Fig. 11c, three PDFs are depicted with different shapes and widths.

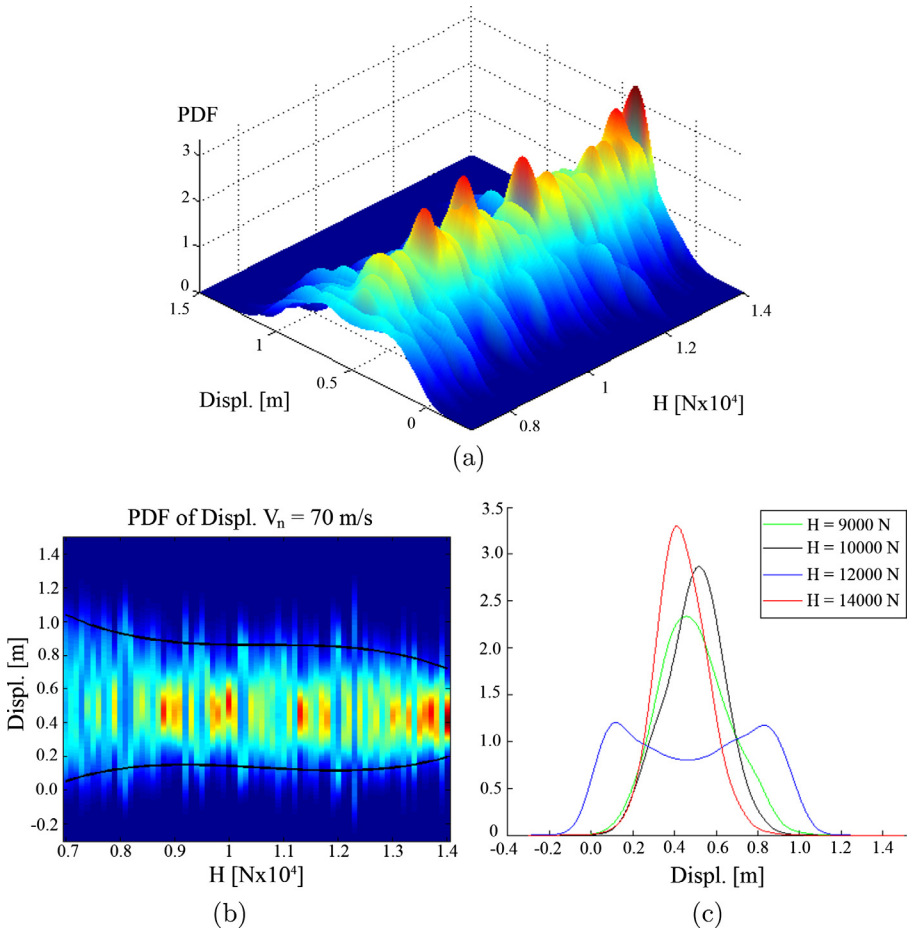

Fig. 10. Evolution of the PDF with H of the transverse displacement of the beam-column at the tip of the mast for $V_n = 70$ m/s and $EI = 1.75 \times 10^8$ N m^2. (a) 3D plot of displacements vs H vs PDF; (b) top view of plot (a); (c) some cuts of plot (a).

The unpredictable behavior and qualitative changes in the PDFs observed in Fig. 11, are associated mainly to the randomness of the wind loads. Different dynamic response results, for each value of V_n, can be expected, since each time record of wind load - associated to a given value of V_n - is different, and this structural typology is very sensitive to the characteristics of the dynamic loading [5]. Then, the origin of the qualitative changes are thought to be associated to a combination of a deterministic bifurcation (as found in [5]) and the so-called phenomenological bifurcation [23] (due the random origin of the load records). The authors believe that both mechanisms of bifurcation are occurring simultaneously, then deeper studies - which are out of the scope of this work - are necessary to properly define the importance of each one on the results.

Fig. 12 illustrates the contour plots of the correlations among the time realizations for all the values of H and four cases of V_n. The warmer color indicates full correlation and the colder color indicates the zero correlation (no anti-correlation is observed). In Fig. 12a (that corresponds to the lowest V_n studied), some good correlation between results in a thin zone around the diagonal can be seen and two larger regions of good correlation for approximately the 30% lowest and highest values of H are present. Fig. 12b has three zones of good correlation, despite the two corresponding to the lowest values of H are very small. Fig. 12c and d depict poor or none correlations among results, even close to the diagonal. For a fixed value of H and for all the cases of V_n, plots like Fig. 12d are obtained. From this analysis, it can be concluded that, for mean to high values of V_n, the shape of the time history of displacements exhibits high sensitivity with V_n and H and the evolution of the results does not follow any linear relationship, even when results for close values of H or V_n are compared.

5.1.1. Probability of exceeding a limit value

The probability that the displacements (D) (all the displacements of each experiment, not exclusively the peaks) exceed a limit value, arbitrarily fixed on $D_{lim} = 0.20$ m, is evaluated for CASE 1. Since the wind load is a stochastic process, the response of the system (the displacement, in this case) is a stochastic process as well. As before, each run is treated as a stochastic process and the probability of exceeding a limit value, is evaluated for each combination of H and V_n (Fig. 13a) and EI and V_n (Fig. 13b) (H, EI and V_n are not considered stochastic in this study). Since each run is a "temporal" experiment, Fig. 13 can be interpreted as well as the percentage of the total runtime that the structure exceeds the limit value. Here, a limit value of 0.20 m that could be an operational limit, is selected. It is noticeable that the variation along a vertical line (a fixed value of V_n and different values of H or EI) is smaller when compared to the obtained on a horizontal line (fixed value of H or EI and different values of V_n). This shows that the influence of the structural parameters H and EI is smaller than V_n on the response, when a specific value (or range) is studied.

5.2. CASE 2. Stochastic wind load. Wind nominal velocity as a stochastic variable and deterministic H, EI

Now, the V_n parameter is considered stochastic. Gumbel and Fréchet PDFs are respectively used to observe the propagation of uncertainty of this parameter over statistics of the peak displace-

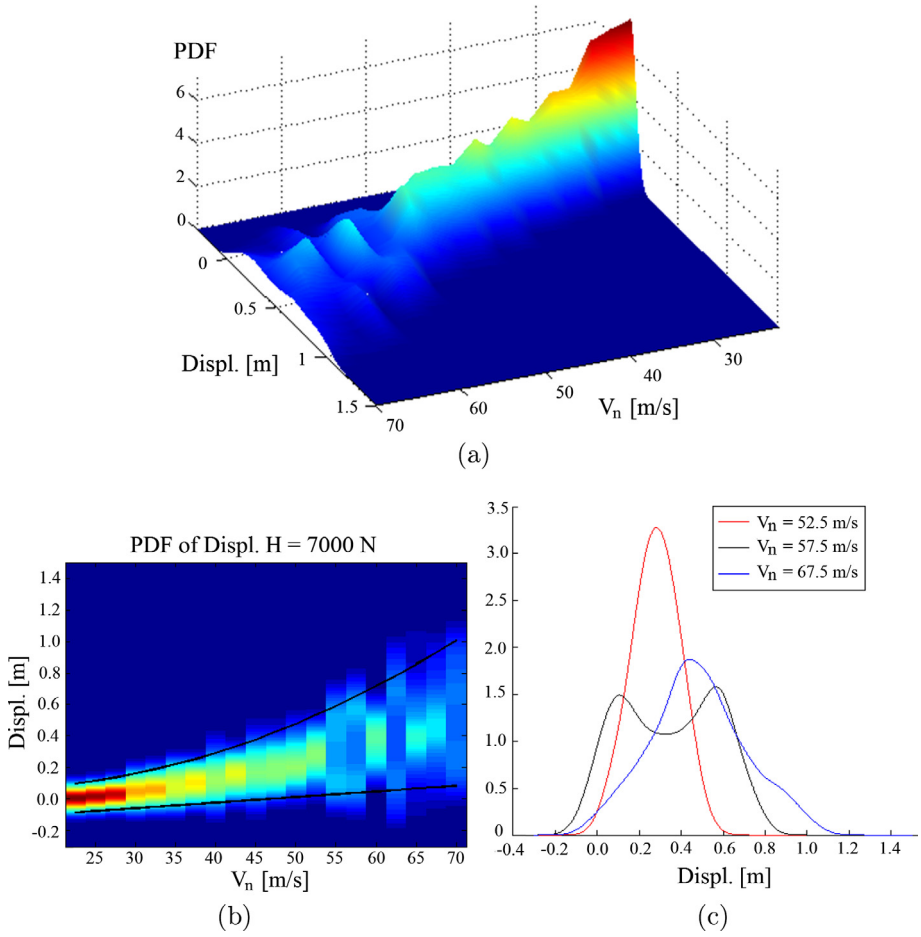

Fig. 11. Evolution of the PDF with V_n of the transverse displacement of the beam-column at the tip of the mast for $H = 7000$ N and $EI = 1.75 \times 10^8$ N m^2. (a) 3D plot of displacements vs V_n vs PDF; (b) top view of plot (a), (c) some cuts of plot (a).

ments. The influence of the *EI* and *H* is also studied, since the statistics of V_n are considered for each individual case of these two variables. Fig. 14 depicts the PDF of the peak displacements at the top of the guyed mast. Fig. 14a and b show the variation of the displacements with the *EI* parameter found with a fixed value of $H = 10.5$ kN. Fig. 14c and d contain similar graphs but varying the value of *H* and for $EI = 1.75 \times 10^8$ N m^2. The effects of using the different PDFs are evident. The PDF of the results using a Gumbel PDF for V_n (Fig. 14a) are more disperse and often multimodalities can be observed (particularly in the third portion corresponding to lower values of *EI*). On the other hand, using a Fréchet distribution for the input random variable (Fig. 14b), the resulting PDF is more compact and gamma shaped; the modes and the PDFs are located in a zone of higher peak displacements values, in agreement with a Fréchet PDF, which have higher probabilities on the zone of higher V_n while the Gumbel distribution have a more distributed probability among all the values of V_n. Yet, the mode corresponding to the higher value of peak displacements in the Gumbel case matches the mode of the Fréchet case (Fig. 14a and b). Then, the prediction of the most dangerous displacements is accomplished similarly in both situations. The difference lies in that a Gumbel PDF yields wider dispersion, since other lower values also have high probabilities of occurrence (Fig. 14a and b).

The *EI* parameter affects the mean and the dispersion, strongly in the first third region of the values of *EI*. Otherwise its influence is reduced, but still present.

An important variation in the PDFs of the results is observed in plots (Fig. 14c and d). In the problem depicted in Fig. 14c, truncated exponential-like PDFs are obtained while gamma-like functions are found in the case reported in Fig. 14d. Despite the variations, no multimodalities are found in the last two problems.

5.3. CASE 3. Stochastic wind load. Guy tension as a stochastic variable and deterministic EI, V_n

Fig. 15 shows plan view graphs for the case of the variable *H* assumed stochastic with three different PDFs with $EI = 1.75 \times 10^8$ N m^2. The change of the wind velocity values leads to some kind of nonlinear variation of the mean/mode of the peak results. On the other hand, some "steps" are observed within the rightmost third. In this region, an increase of the wind velocity does not correspond to an increase of the mode or a change in the shape of the peak displacements distribution. The choice of the PDF of *H* has a small influence on the results, which indicates that the another source of randomness (the load) has a predominant influence on the statistic results.

Next, a gamma PDF is used to describe *H*. Plan views of the statistic results obtained with the stochastic variable *H* and two different wind velocities are depicted in Fig. 16. The PDFs of the peak displacements are shown for $V_n = 55$ and 60 m/s, resp. and for two standard deviation values for *H* (*i.e.*, 0.05 H_m and 0.025 H_m, resp.). A unexpected outcome is that when the dispersion of *H* is reduced and the PDF has values more clustered closely to the mean, a larger number of multimodalities are present in the results. The mode values behave as expected in a rather nonlinear fashion. The changes with the velocity (from 55 m/s to

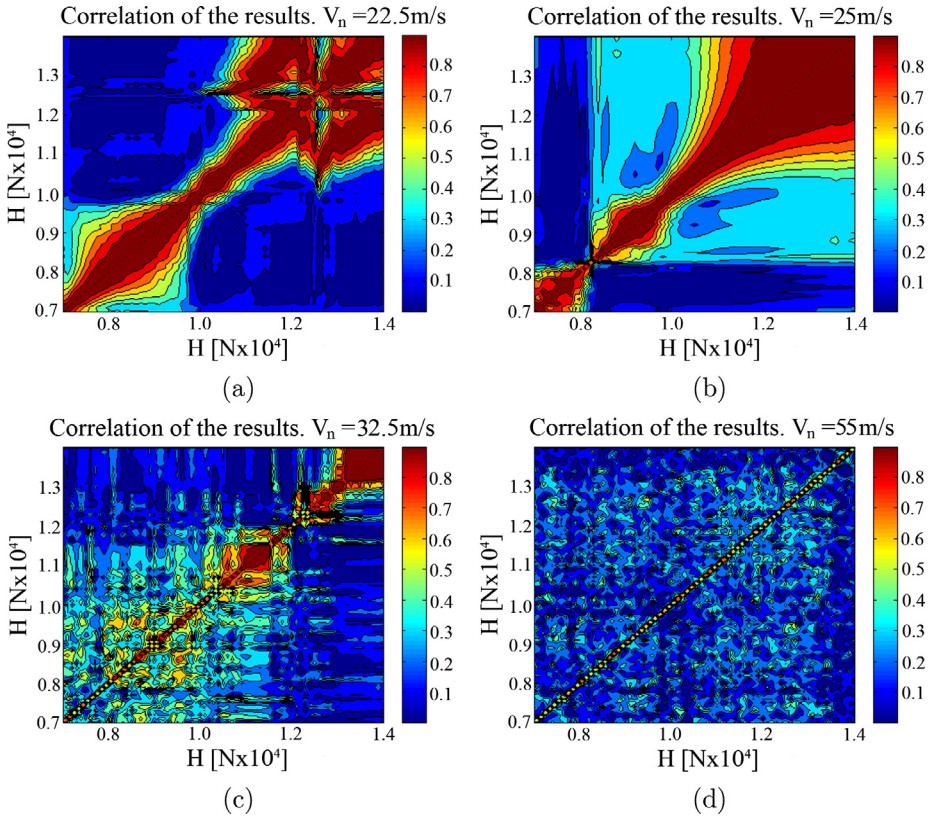

Fig. 12. Correlation of the transverse displacement of the beam-column at the tip of the mast found with the deterministic reduced order model for all the combinations of H and four cases of V_n.

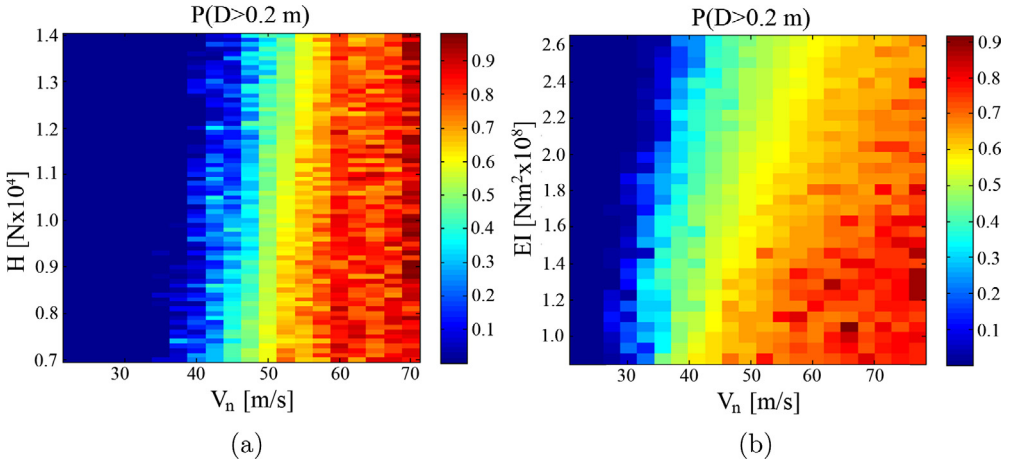

Fig. 13. Exceeding of the limit value of 0.2 m at the tip of the mast. (a) Percentage of time that the transverse displacement of the beam-column exceeds the limit value at at the tip of the mast for all the combinations of H and V_n; (b) Probability that the displacements exceed a limit value for all combinations of EI and V_n.

60 m/s) exhibit a significant variation for a small variation of the wind velocity. When other results found with different input PDFs (*e.g.* uniform PDF) are plotted, similar effects are observed. More disperse distributions yield more homogeneous results, *i.e.*, less variable among the different values of $E[H]$ and unimodality. However, the use of more concentrated PDFs, leads to more variable modes among the $E[H]$ and frequently, bimodalities are present. The higher the wind velocities, the more visible the effects.

5.4. CASE 4. Stochastic wind load. Stiffness of the mast as stochastic variable and deterministic H, V_n

Here, the EI parameter is considered stochastic. A uniform PDF, a truncated exponential PDF and a gamma PDF are respectively used to observe the propagation of uncertainty of this parameter over the local peak displacements statistics. The influence of the V_n is also studied, since the statistics using EI as stochastic parameter are assessed for each individual case of V_n.

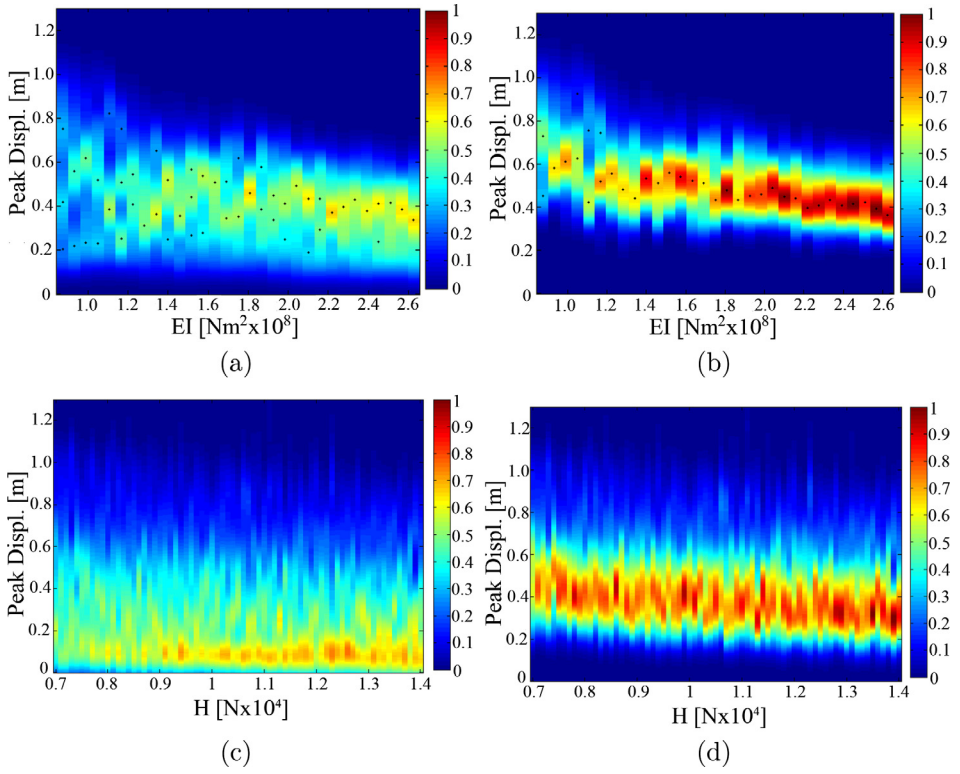

Fig. 14. Plan views of the PDFs of peak displacements using V_n with distributions Gumbel and Fréchet. (a) Variation with EI (V_n represented by a Gumbel PDF) for H = 10,500 N; (b) variation with EI (V_n represented by a Fréchet PDF) for H = 10,500 N; (c) variation with H (V_n represented by a Gumbel PDF) for $EI = 1.75 \times 10^8$ N m^2; (d) variation with H (V_n represented by a Fréchet PDF) for $EI = 1.75 \times 10^8$ N m^2.

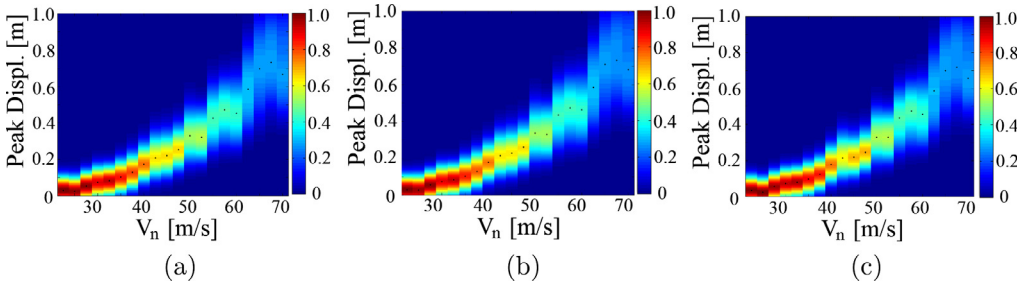

Fig. 15. Plan views of the PDFs of peak displacements for each value of V_n, $EI = 1.75 \times 10^8$ N m^2 and stochastic cable pretension H with distributions: (a) uniform; (b) truncated exponential; (c) gamma.

Fig. 17 depicts a plan view of the PDF of the peak displacements at the top of the guyed mast. Each vertical strip corresponds to a case of V_n. The warmer colors indicate higher probability (and also the location of the modes) while the colder colors indicate the opposite. All the resulting distributions are gamma-like PDFs and the mean and the mode mostly coincide. No differences can be seen when using a uniform PDF or a truncated exponential PDF in the PDF of the results. Instead, the gamma PDF exhibits a smaller dispersion in the results. Nevertheless, the differences are small and it seems that the choice of the PDF for EI does not affect significantly the statistics of the peak displacements. Again, this indicates (as seen in CASE 3) that the stochasticity of the load exhibits a predominant influence, that makes opaque the importance of the structural parameters studied. The V_n parameter seems to influence the mode and dispersion in a linear fashion (specific figures are not provided for sake of brevity).

5.5. CASE 5. Stochastic wind load. Wind nominal velocity and stiffness of the mast as random variables. Deterministic H

Next, both EI and V_n are considered stochastic together. The resulting PDFs of peak displacements are depicted in Fig. 18. Again, the influence of the PDF of EI is small in the PDFs of peak displacements. For the case of Fréchet PDF, the result is more compact than the case of a Gumbel PDF. In this study, no multimodalities are observed and the modes do not match, being the more conservative results the ones corresponding to the Fréchet PDF.

5.6. CASE 6. Stochastic wind load. Guy tension and nominal wind velocity as stochastic variables. Deterministic bending mast stiffness EI

The cable pretension and the wind velocity were considered jointly stochastic (H and V_n). Fig. 19 includes the plots obtained by changing the PDFs of H (uniform, truncated exponential and

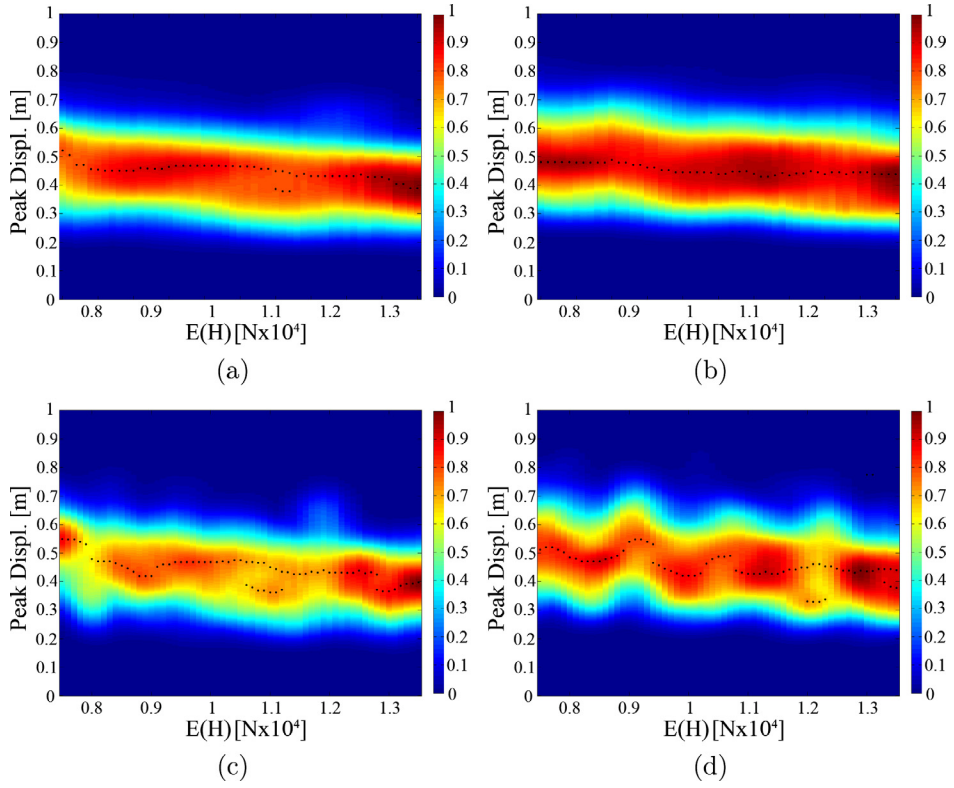

Fig. 16. Plan views of the PDF of peak displacements found with H (gamma distribution). (a) Wind velocity $V_n = 55$ m/s; $\sigma_H = 0.05H_m$; (b) wind velocity $V_n = 60$ m/s; $\sigma_H = 0.05H_m$; (c) wind velocity $V_n = 55$ m/s; $\sigma_H = 0.025H_m$; (d) wind velocity $V_n = 60$ m/s; $\sigma_H = 0.025H_m$.

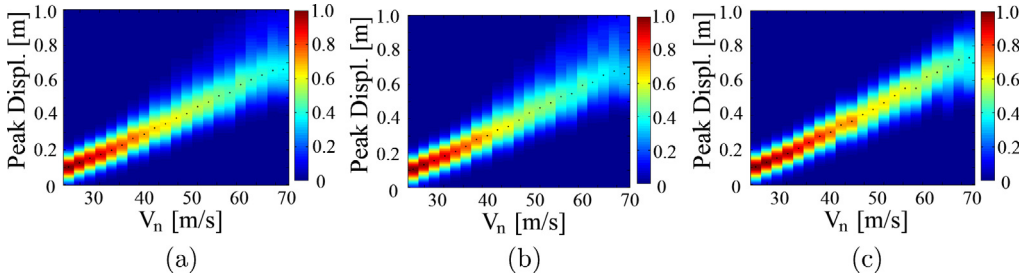

Fig. 17. Plan views of the PDFs of peak displacements for each value of V_n for H = 10,500 N, using the mast stiffness EI as stochastic variable with distributions: (a) uniform; (b) truncated exponential; (c) gamma.

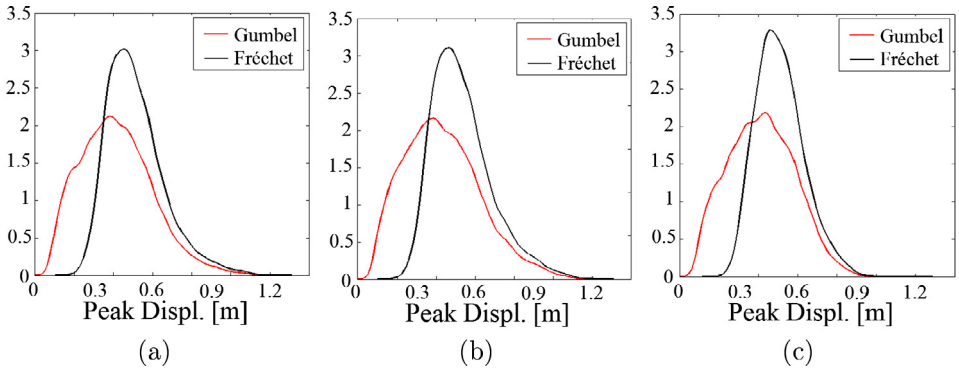

Fig. 18. PDF of peak displacements using EI and V_n as joint stochastic variables. Each subfigure plots both the cases of Fréchet and Gumbel PDFs for V_n. PDF of EI: (a) uniform; (b) truncated exponential; (c) gamma.

gamma, resp.) and two PDFs for the wind velocity (Gumbel and Fréchet, resp.). Similarly to the trend observed in Fig. 18 in which the stochastic variables were EI and V_n, the choice of the PDF for the structural parameter does not affect the results. With the Gumbel PDF, truncated exponential-like functions are obtained while gamma-shaped are found with the Fréchet PDF. Despite the input PDF of H or EI seems to have small effects on the results depicted in Figs. 18 and 19, it can be seen that the choice of the

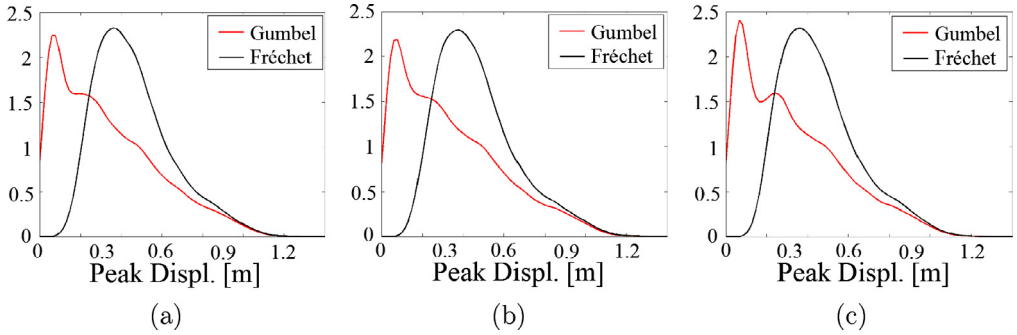

Fig. 19. PDF of peak displacements using V_n and EI as joint stochastic variables. V_n is represented with Fréchet and Gumbel PDFs resp. H is represented by: (a) uniform PDF; (b) truncated exponential; (c) gamma.

random variable is indeed relevant when the nominal wind velocity is represented by a Gumbel PDF (*cf.* the red curve in both figures). The latter is the PDF in use in most of the codes. On the contrary, the Fréchet curves remain similar regardless the cable pretension or the mast bending stiffness are considered random.

6. Concluding remarks

A model of a guyed mast (beam-column and one guy) under dynamic wind load was mathematically stated. The governing equations result nonlinear due to the cable formulation. The wind load was described within a stochastic framework through the Spectral Representation Method. Additionally, the structural model was also considered stochastic through the inclusion of random structural parameters. In order to perform the Monte Carlo simulations, a reduced order model was stated, using a basis of natural mode shapes. A stochastic analysis was then carried out for different cases including the consideration of the stochastic wind load and, additionally, random parameters as the nominal wind velocity V_n, the guy tension H and the mast bending stiffness EI, separately or in combinations. Three probability density distributions (PDF) were chosen to describe H and EI, which were deduced from the Principle of Maximum Entropy. Meanwhile, V_n was described by the Gumbel and Fréchet distributions.

After the uncertainty quantification, it was found that the influence of the variables on the dynamic response of the guyed mast is diverse. It was found that the randomness of the load is the strongest source of uncertainty in the statistics of the results. When the structural parameters are also considered stochastic (all the studies were performed with the random wind load), it was found that, under the various studied distributions, the PDFs of the peak displacements were similar. This means that the wind load has a higher influence on the statistic response than the randomness of the structural parameters. The characteristics of the resulting PDFs of peak displacements when H or EI are considered stochastic, are highly influenced by the nominal wind velocity (V_n). For the highest values of V_n, qualitative changes in the PDFs occur within a small range of V_n, which includes a fast increase in the dispersion and the occurrence of multimodalities. Also, it was found that when lower dispersion values are used for the PDF of H the resulting PDFs are more sensitive to $E(H)$ and multimodalities and bifurcation of the PDFs are also observed within small ranges of $E(H)$. When the nominal wind velocity was assumed stochastic on top of the random signal, it was found that the use of a Gumbel PDF gives more disperse results. When the Fréchet PDF is used, more concentrated PDFs are obtained, with the modes placed near the highest values of displacements, which indicates that the results are more conservative.

From the above study, it can be concluded that the guy tension and the nominal wind velocity appear to be the two most influential parameters on the dynamic response, unlike the bending stiffness. Thus, cautious maintenance schedules should be carried out in guyed structures to ensure the smaller possible variability of the guy pretension and to avoid the large variation of the results. Finally, it is apparent that the stochastic modeling and the uncertainty quantification contribute to obtain a more realistic description of the problem and to bring out the sensitivity of the structural system to a given parameter in a comprehensive way.

Acknowledgments

The authors acknowledge the financial support from CONICET, MINCyT and UNS (Argentina); CAPES, CNPq, and FAPERJ (Brazil). The third author is grateful to Prof. Giuseppe Rega for his knowledgeable advices regarding the structural model.

Appendix A

The constants of Eqs. (5) and (6) are listed next. For the sake of brevity, a compact notation is introduced. For instance, if one needs to calculate d_{211} then, as stated in the fourth line, $L^2 = d$ and afterwards, in the sixth line, L^i_{jkk} with $i=2$, $j=2$ and $k=1$, gives $L^2_{211} = d_{211}$.

$$\bar{m}_i = m_b \int_0^{L_b} \phi^{\prime 2}_{b_v i} + \phi^{\prime 2}_{b_u i} dx_b + m_c \int_0^{L_c} \phi^{\prime 2}_{c_v i} + \phi^{\prime 2}_{c_u i} dx_c, \quad (i=1,2).$$

$$\bar{a}_i = c_b \int_0^{L_b} \phi^{\prime 2}_{b_v i} + \phi^{\prime 2}_{b_u i} dx_b + c_c \int_0^{L_c} \phi^{\prime 2}_{c_v i} + \phi^{\prime 2}_{c_u i} dx_c, \quad (i=1,2).$$

$$\bar{p}_i = \int_0^{L_b} P_{b_v i}\phi_{b_v i} + P_{b_u i}\phi_{b_u i} dx_b + \int_0^{L_c} P_{c_v i}\phi_{c_v i} + P_{c_u i}\phi_{c_u i} dx_c, \quad (i=1,2).$$

$$L^1 = \bar{c}, \quad L^2 = \bar{d}.$$

$$L^i_{kkk} = \frac{1}{2} EA_c \int_0^{L_c} \phi^{\prime 3}_{c_v k} \phi^{\prime}_{c_v i} d(x_c), \quad (k=1,2;\ i=1,2).$$

$$L^i_{jkk} = \frac{3}{2} EA_c \int_0^{L_c} \phi^{\prime 2}_{c_v k} \phi^{\prime}_{c_u j} \phi^{\prime}_{c_v i} d(x_c), \quad (k=1,2;\ j=1,2;\ k \neq j;\ i=1,2).$$

$$L^i_i = \int_0^{L_b} EI\phi^{\prime\prime 2}_{b_v i} + EA_b \phi^{\prime 2}_{b_u i} dx_b + \int_0^{L_c} H\phi^{\prime 2}_{c_v i} + EA_c \phi^{\prime 2}_{c_u i} + 2EA_c Y^{\prime}_c \phi^{\prime}_{c_u i}\phi^{\prime}_{c_v i} + 2EA_c Y^{\prime 2}_c \phi^{\prime 2}_{c_v i} dx_c, \quad (i=1,2).$$

$$L^i_j = \int_0^{L_c} EA_c (Y^{\prime}_c \phi^{\prime}_{c_u j}\phi^{\prime}_{c_v i} + Y^{\prime 2}_c \phi^{\prime}_{c_v j}\phi^{\prime}_{c_v i} + \phi^{\prime}_{c_v j}\phi^{\prime}_{c_u i}) dx_c, \quad (j=1,2;\ i=1,2;\ i \neq j).$$

$$L^i_{12} = \int_0^{L_c} EA_c (3Y^{\prime}_c \phi^{\prime}_{c_v 1}\phi^{\prime}_{c_v 2}\phi^{\prime}_{c_v i} + \phi^{\prime}_{c_u 1}\phi^{\prime}_{c_v 2}\phi^{\prime}_{c_v i} + \phi^{\prime}_{c_u 2}\phi^{\prime}_{c_v 1}\phi^{\prime}_{c_v i} + Y^{\prime}_c \phi^{\prime}_{c_v 1}\phi^{\prime}_{c_v 2}\phi^{\prime}_{c_u i}) dx_c, \quad (i=1,2).$$

$$L^i_{jj} = \int_0^{L_c} EA_c \left(\frac{3}{2} Y^{\prime}_c \phi^{\prime 2}_{c_v j}\phi^{\prime}_{c_v i} + \phi^{\prime}_{c_v j}\phi^{\prime}_{c_u j}\phi^{\prime}_{c_v i} + \frac{1}{2}\phi^{\prime 2}_{c_v j}\phi^{\prime}_{c_u i} \right) dx_c, \quad (j=1,2;\ i=1,2).$$

References

[1] Preidikman S, Massa J, Roccia B. Análisis dinámico de mástiles arriostrados. Rev Int Desastres Nat, Accid Infraestruct Civil 2006;6(1):85–102.
[2] Shi H. Nonlinear finite element modeling and characterization of guyed towers under severe loading [Ph.D. thesis]. Columbia: University of Missouri; 2007.

[3] de Oliveira MI, da Silva JG, da S. Vellasco PC, de Andrade SA, de Lima LR. Structural analysis of guyed steel telecommunication towers for radio antennas. J Br Soc Mech Sci Eng 2007;29:185–95.
[4] Saudi G. Structural assessment of a guyed mast through measurement of natural frequencies. Eng Struct 2014;59:104–12.
[5] Lenci S, Ruzziconi L. Nonlinear phenomena in the single mode dynamics of a cable-supported beam. Int J Bifurcat Chaos 2009;19:923–45.
[6] Wei MH, Xiao YQ, Liu HT. Bifurcation and chaos of a cable–beam coupled system under simultaneous internal and external resonances. Nonlinear Dyn 2011;67(3):1969–84.
[7] Wei M, Lin K, Jin L, Zou D. Nonlinear dynamics of a cable-stayed beam driven by sub-harmonic and principal parametric resonance. Int J Mech Sci 2016;110:78–93.
[8] Wang Z, Sun C, Zhao Y, Yi Z. Modeling and nonlinear modal characteristics of the cable-stayed beam. Eur J Mech - A/Solids 2014;47:58–69.
[9] Bellizzi S, Sampaio R. Reduced models based on smooth decomposition for random mechanical systems. Int Rev Mech Eng 2012;6(1):74–85.
[10] Margariti G, Gantes C. Linear and nonlinear buckling response and imperfection sensitivity of cable-stayed masts and pylons. Struct Eng Int 2015;25(1):43–9.
[11] Shinozuka M, Jan C. Digital simulation of random processes and its applications. J Sound Vib 1972;25(1):111–28.
[12] Dyrbye C, Hansen S. Wind loads on structures. 1st ed. West Sussex, England: John Willey and Sons; 1994.
[13] Miguel L, Fadel Miguel L, Riera J, Kaminski Jr J, Menezes R. Assessment of code recommendations through simulation of EPS wind loads along a segment of a transmission line. Eng Struct 2012;43:1–11.
[14] Gattulli V, Lepidi M. Localization and veering in the dynamics of cable-stayed bridges. Comput Struct 2007;85:1661–78.
[15] Shi H, Salim H. Geometric nonlinear static and dynamic analysis of guyed towers using fully nonlinear element formulations. Eng Struct 2015;99:492–501.
[16] ALGOR. ALGOR V23.01. Professional MES; 2009.
[17] CIRSOC-INTI. Standard CIRSOC 102. Wind actions on constructions. INTI, Buenos Aires, Argentina; 2005 [in Spanish].
[18] Shannon C. A mathematical theory of communication. Bell Tech J 1948;27:379–423.
[19] Cursi E, Sampaio R. Uncertainty quantification and stochastic modeling with matlab. 1st ed. Elsevier; 2015.
[20] Kapur JN, Kesavan HK. Entropy optimization principles and their applications. Springer; 1992.
[21] CIRSOC-INTI. Standard CIRSOC 306. Steel Structures for antennas. INTI, Buenos Aires, Argentina; 1995 [in Spanish].
[22] Ballaben JS, Rosales M, Sampaio R. Stochastic dynamics of a non-linear cable-beam system. J Br Soc Mech Sci Eng 2016;38(1):307–16.
[23] Zakharova A, Vadivasova T, Anishchenko V, Koseska A, Kurths J. Stochastic bifurcations and coherencelike resonance in a self-sustained bistable noisy oscillator. Phys Rev E 2010;81:1–6.